Interplay between Fe and Nd magnetism in NdFeAsO single crystals

W. Tian,[1] W. Ratcliff II,[2] M. G. Kim,[1,3] J.-Q. Yan,[1] P. A. Kienzle,[2] Q. Huang,[2] B. Jensen,[1] K. W. Dennis,[1] R. W. McCallum,[1,4] T. A. Lograsso,[1] R. J. McQueeney,[1,3] A. I. Goldman,[1,3] J. W. Lynn,[2] and A. Kreyssig[1,3]

[1]*Ames Laboratory, Ames, Iowa 50011, USA*
[2]*NIST Center for Neutron Research, National Institute of Standards and Technology, Gaithersburg, Maryland 20899, USA*
[3]*Department of Physics and Astronomy, Iowa State University, Ames, Iowa 50011, USA*
[4]*Department of Materials Science and Engineering, Iowa State University, Ames, Iowa 50011, USA*

(Dated: June 6, 2010)

The structural and magnetic phase transitions have been studied on NdFeAsO single crystals by neutron and x-ray diffraction complemented by resistivity and specific heat measurements. Two low-temperature phase transitions have been observed in addition to the tetragonal-to-orthorhombic transition at $T_S \sim 142\,\mathrm{K}$ and the onset of antiferromagnetic (AFM) Fe order below $T_N \sim 137\,\mathrm{K}$. The Fe moments order AFM in the well-known stripe-like structure in the (**ab**) plane, but change from AFM to ferromagnetic (FM) arrangement along the **c** direction below $T^* \sim 15\,\mathrm{K}$ accompanied by the onset of Nd AFM order below $T_{\mathrm{Nd}} \sim 6\,\mathrm{K}$ with this same AFM configuration. The iron magnetic order-order transition in NdFeAsO accentuates the Nd-Fe interaction and the delicate balance of **c**-axis exchange couplings that results in AFM in LaFeAsO and FM in CeFeASO and PrFeAsO.

PACS numbers: 74.70.Xa, 75.25.-j, 61.50.Ks, 75.30.Kz

Since the discovery of high-temperature superconductivity in the fluorine-doped compound $LaFeAsO_{1-x}F_x$ with a superconducting transition temperature of $T_c = 26\,\mathrm{K}$[1], enormous efforts have been made to understand the crystallographic, magnetic, and superconducting properties of the RFeAsO compounds (R = rare earth elements) and their doped superconducting derivatives with T_cs up to $\sim 55\,\mathrm{K}$[2,3,4,5,6,7,8,9,10,11,12,13,14,15,16]. The parent RFeAsO compounds undergo a tetragonal-to-orthorhombic phase transition and show antiferromagnetic (AFM) order of Fe and R moments[2,12,13,14,15]. Although doping suppresses both the lattice distortion and Fe magnetic order, magnetism is believed to play a major role in the superconducting pairing mechanism in pnictide superconductors demonstrated, e. g., by the observation of a magnetic resonance in the superconducting state[17]. Detailed knowledge of the magnetic order and crystallographic structure is key to gaining insight into the magnetic and magneto-elastic coupling, but has been hampered, so far, by the absence of sizeable RFeAsO single crystals.

Here we report on a neutron and x-ray diffraction study of recently available[18] NdFeAsO single crystals complemented by resistivity and specific heat measurements. In prior neutron powder studies, the tetragonal-to-orthorhombic lattice distortion has been observed below $T_S \sim 150\,\mathrm{K}$[13] followed by the onset of the well-known stripe-like AFM order of Fe below $T_N \sim 141\,\mathrm{K}$[12]. The onset of the Nd AFM order was reported for temperatures below $T_{\mathrm{Nd}} \sim 2\,\mathrm{K}$ in the neutron powder diffraction experiment[13]. However, resistivity[19] and muon-spin relaxation[20] studies indicate a low-temperature phase transition at 5-6 K. Our NdFeAsO single crystals show two low-temperature transitions in addition to the high-temperature transitions at $T_S \sim 142\,\mathrm{K}$ and $T_N \sim 137\,\mathrm{K}$. Below $T^* \sim 15\,\mathrm{K}$, the Fe moments undergo a strongly hysteretic magnetic transition from AFM arrangement to a ferromagnetic (FM) arrangement along the **c** direction. The Nd moments order AFM below $T_{\mathrm{Nd}} \sim 6\,\mathrm{K}$, coupled to the Fe magnetic order by a common magnetic propagation vector, indicating a complex interplay between Nd and Fe magnetism.

NdFeAsO single crystals were grown out of NaAs flux as described in Ref. 18. Batches with mm-sized single crystals and masses up to 7 mg were carefully examined by wavelength dispersive spectroscopy and x-ray powder diffraction. Different samples from the same batch show no significant deviations in their stoichiometry. No impurity phases were detected beyond the NaAs flux. Specific heat and resistivity were measured in a Quantum Design Physical Property Measurement System[21] by the relaxation method and the four-probe technique using Epotek H20E silver epoxy contacts on platinum leads. The homogeneity of the batches was examined by resistivity measurements of several single crystals showing similar behavior. The reproducibility and excellent homogeneity of the grown material were additionally confirmed by neutron diffraction measurements on polycrystalline samples consisting of more than 300 crystals. They showed well-defined transition temperatures and Bragg peaks in excellent agreement with the single crystal measurements reported here. To check potential ferromagnetism, the magnetization, M, was measured with increasing temperature from 5 to 20 K for eleven fields, H, between 0.1 and 5 T and the differential susceptibility was calculated at each temperature. Parallel to the **c** axis, the zero-field intercept of the M vs H line characterizing a FM component was essentially temperature independent giving an upper limit of $0.012\,\mu_B$/formula unit. Perpendicular to the **c** axis the value was an order of magnitude smaller.

The lattice distortion was characterized by high-resolution x-ray diffraction measurements using a four-circle diffractometer and Cu-$K_{\alpha 1}$ radiation from a rotat-

ing anode x-ray source, selected by a Ge(1 1 1) monochromator. The plate-like single crystal was attached to a flat copper sample holder on the cold finger of a closed-cycle displex refrigerator. A mosaicity of ~ 0.03 deg was determined from full width at half maximum of the rocking curve of the (0 0 6) Bragg peak. The orthorhombic distortion, δ, was determined as described in Ref. 22 using $(\xi\,\xi\,0)$ scans through the tetragonal (1 1 7) Bragg peak which splits into the orthorhombic (2 0 7) and (0 2 7) Bragg peaks below T_S.

The neutron diffraction experiments were carried out using the BT9 thermal neutron triple-axis spectrometer at NCNR, NIST. The crystal was mounted on a thin aluminum post, oriented in the orthorhombic $(h\,0\,l)$ scattering plane, and placed in an ILL cryostat. Rocking scans were resolution limited, indicating the high quality of the sample. Neutrons with a fixed incident energy of 14.7 meV and a collimation of 40'-48'-sample-40'-open were used. Additional measurements were taken on a number of crystals heat treated in various ways to check the results, and the observed transitions were all consistent with uncertainties, which are statistical and represent one standard deviation. Descriptions are given in terms of the orthorhombic crystallographic (nuclear) unit cell present below T_S.

In Fig. 1, we compare the four measurements as a function of temperature. The anomaly at $T_S \sim 142$ K in specific heat and resistivity measurements correlates with the phase transition from tetragonal $P\,4/n\,m\,m$ to orthorhombic $C\,m\,m\,a$. The orthorhombic lattice distortion, δ, increases below T_S for decreasing temperature without further anomalies. Figure 2(a) shows the splitting of the tetragonal (2 2 0) Bragg peak into the orthorhombic (4 0 0) and (0 4 0) Bragg peaks from our high-resolution neutron diffraction measurements and demonstrates the bulk nature of the lattice distortion and the homogeneity of the sample, through resolution-limited peak shapes and a uniform transition temperature.

The second anomaly found in specific heat and resistivity data at $T_N \sim 137$ K corresponds to the onset of the well-known AFM stripe-like Fe order with AFM arrangement between nearest neighbors in **a** and **c** direction and FM along the **b** direction[12]. The intensity of the magnetic (1 0 3/2) Bragg peak increases below T_N [see Fig. 1(d)]. The inset illustrates that this transition shows no hysteresis upon cooling and warming through T_N consistent with a second order transition.

At low temperature, a weak and broad anomaly in the resistivity can be associated with the disappearance of the magnetic (1 0 3/2) Bragg peak at $T^* \sim 15$ K signaling a change in the Fe magnetic order. This behavior is demonstrated in Fig. 2(c) by rocking scans through the (1 0 3/2) peak at selected temperatures. At the same temperature, T^*, new magnetic Bragg peaks occur as illustrated in Fig. 2(b) by the (1 0 1) peak and in Fig. 1(d) by the (1 0 0) peak. The intensity of these peaks increases with decreasing temperature as the Fe order changes, while below $T_{\rm Nd} \sim 6$ K the increase is much more pronounced. At $T_{\rm Nd}$, a sharp peak is also observed in the specific heat [see inset of Fig. 1(a)] and the temperature derivative of the resistivity indicating the onset of the Nd magnetic order.

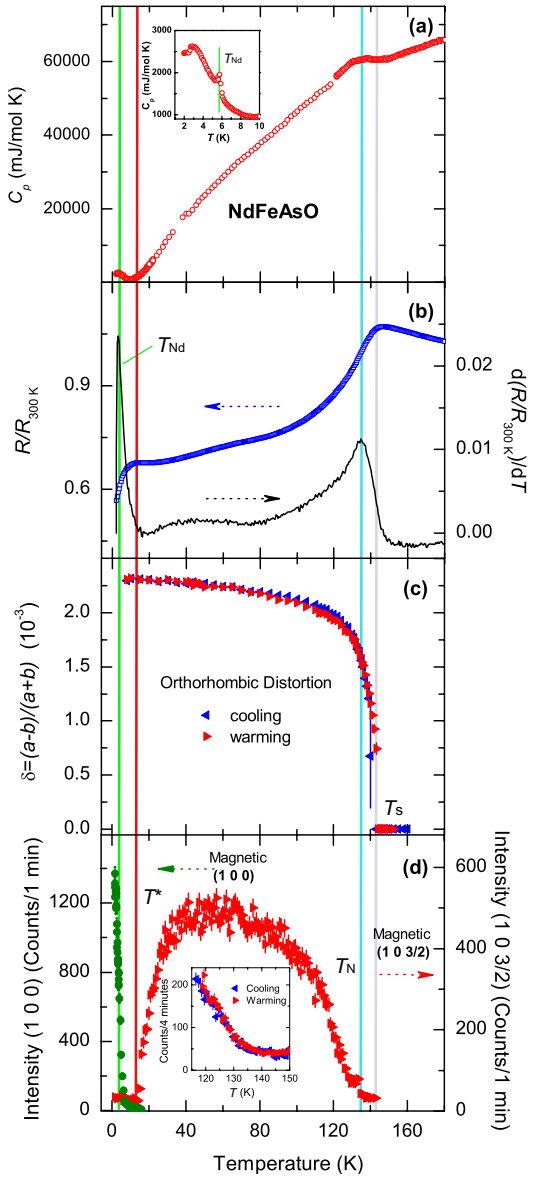

FIG. 1: (Color online) (a) Temperature dependence of the specific heat. (b) resistivity (open symbol, left axis) and its derivative (line, right axis). (c) Orthorhombic distortion, δ, determined by x-ray diffraction as described in the text. (d) Neutron peak intensity for the magnetic Bragg peaks at (1 0 0) (left axis) and at (1 0 3/2) (right axis). The insets show expanded scales.

Details of the temperature dependence for these low-temperature transitions are shown in Fig. 3. The transition at $T^* \sim 15$ K shows hysteretic behavior illustrated in Fig. 3(b), through the temperature dependence of the magnetic (1 0 3/2) and (1 0 1) Bragg peaks (corresponding to the high- and low-temperature phases, respec-

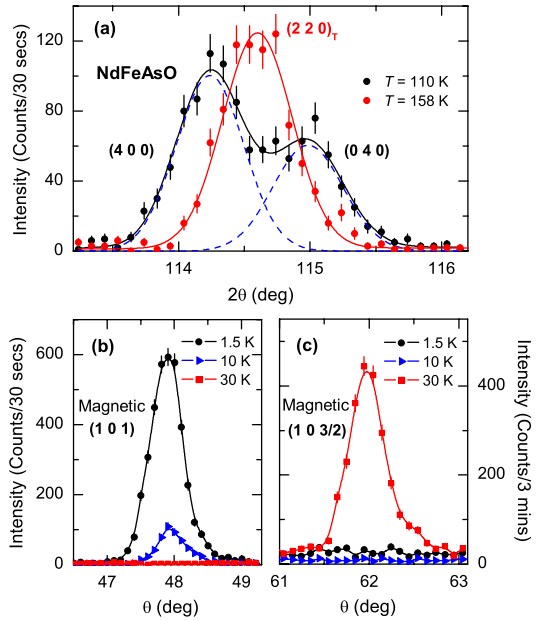

FIG. 2: (Color online) (a) Neutron diffraction θ-2θ scans through the tetragonal (2 2 0) nuclear Bragg peak at $T = 158\,\mathrm{K}$ and its splitting into two orthorhombic Bragg peaks at $T = 110\,\mathrm{K}$ measured with reduced collimation of 10'-10'-sample-10'-10'. Neutron diffraction rocking scans through the magnetic Bragg peaks at (b) (1 0 1) and (c) (1 0 3/2) at selected temperatures.

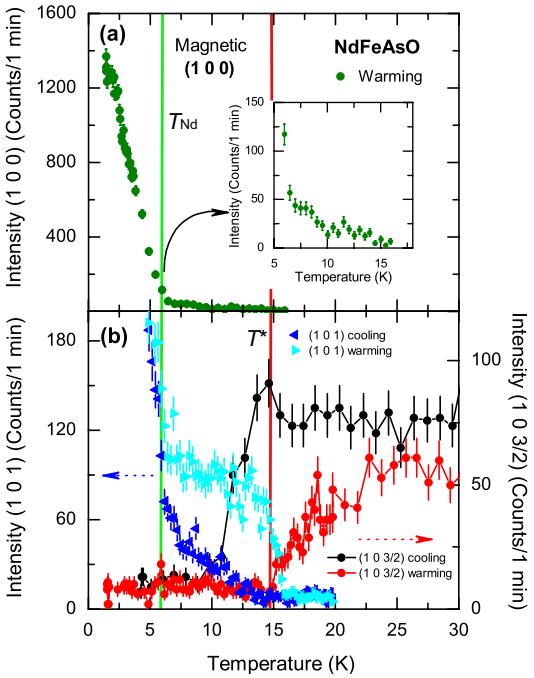

FIG. 3: (Color online) Neutron peak intensity for the magnetic Bragg peaks at (a) (1 0 0) and (b) at (1 0 1) (left axis) and (1 0 3/2) (right axis). The inset in (a) shows an expanded scale between T_{Nd} and T^*.

tively). The strong hysteresis of approx. 3 K points to the first order character of this transition at T^*. As illustrated in Fig. 3, the (1 0 0) and (1 0 1) Bragg peaks follow the same trend with (i) weak intensity between T^* and T_{Nd}, and (ii) a strong but smooth and monotonic intensity increase below T_{Nd} without reaching saturation down to the lowest measured temperature of 1.5 K. Both low-temperature transitions are reminiscent of Nd_2CuO_4 ($T_N \sim 280\,\mathrm{K}$), where the Nd-Cu coupling leads to abrupt changes in the Cu spin structure at 76 and 30 K along with a significant induced Nd moment, before the Nd spontaneously order below $\sim 2\,\mathrm{K}$[27,28,29]. It will be interesting to determine theoretically if a similar type of Fe-Nd coupling is the origin of this behavior in NdFeAsO.

For the determination of the magnetic structures, a series of magnetic Bragg reflection intensities were measured by rocking scans at $T = 30\,\mathrm{K}$, 10 K, and 1.5 K. At $T^* < T = 30\,\mathrm{K} < T_N$ we find the AFM structure consistent with the previous report[12]. Fe moments of $0.54(1)\,\mu_B$ are collinearly aligned along the **a** axis with AFM arrangement in the **a** and **c** directions and FM in the **b** direction as illustrated in Fig. 4(a). The magnetic unit cell for this magnetic structure is doubled along the **c** direction with respect to the orthorhombic crystallographic (nuclear) unit cell and yields the observed magnetic Bragg peaks at positions indexed by a propagation vector of (1 0 1/2).

The magnetic diffraction pattern at $T_{\mathrm{Nd}} < T = 10\,\mathrm{K} < T^*$ can be indexed using a magnetic unit cell identical to the orthorhombic crystallographic (nuclear) unit cell. In particular, no doubling along the **c** direction is now required, signaling a change from AFM ordering in this direction above T^* to FM ordering below T^*. Together with the unchanged stripe-like order in the (**ab**) plane, this magnetic structure is simply described by a propagation vector of (1 0 0) and is illustrated in Fig. 4(b). The intensity of all measured magnetic Bragg peaks can still be fit by Fe moments alone with a reduced moment value of $0.32(2)\,\mu_B$ collinearly aligned along the orthorhombic **a** axis.

At $T = 1.5\,\mathrm{K} < T_{\mathrm{Nd}}$ the description of the magnetic diffraction pattern requires both Fe and Nd moments to be ordered, consistent with the strongly enhanced intensity of the magnetic Bragg peaks. While traditional non-linear least-square fits were used to determine the magnetic structure at temperatures above T_{Nd}, below T_{Nd} a maximum likelihood approach was used due to the possibility of strong correlations between parameters and multiple minima. We used the DREAM[23] package to globally explore the parameter space and to determine error estimates on the parameters. We adopted a model with two Nd moments constrained to the same value, but allowed to vary in direction. As with the higher temperatures, the magnitude of the Fe moment was allowed to vary, however the direction was fixed along the **a** axis. We found a unique minimum (modulo symmetry relations) in which the Fe moments have a magnitude of $0.41(5)\,\mu_B$, whereas the Nd moment is $1.30(5)\,\mu_B$. From the analysis of 12 symmetry-independent magnetic Bragg

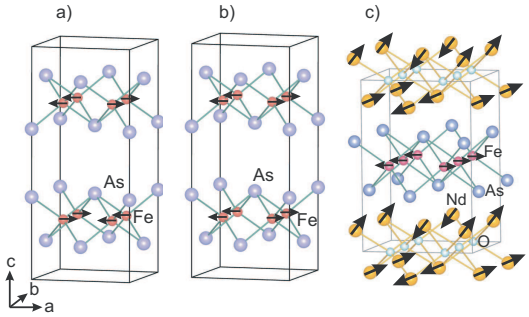

FIG. 4: (Color online) Sketches for the different magnetic structures as described in the text.

peaks, the most likely arrangement consists in magnetic Nd moment vectors $[0.52(8)\ 1.04(4)\ 0.56(10)]\,\mu_B$ and $[1.21(6)\ 0.28(4)\ 0.37(7)]\,\mu_B$ at the atomic positions (0 1/4 0.6389) and (0 3/4 0.3611), respectively. The resulting magnetic structure is illustrated in Fig. 4(c).

Summarizing, below $T_N \sim 137\,\mathrm{K}$, the Fe moments order AFM with the ubiquitous stripe-like arrangement in the orthorhombic (**ab**) plane. For $T < T^* \sim 15\,\mathrm{K}$ the **c** axis configuration changes from AFM as observed in LaFeAsO[2] to FM as found in CeFeAsO[24] and PrFeAsO[25,26]. This temperature dependent change in the Fe magnetic order in NdFeAsO is unique in the *R*FeAsO series and demonstrates that the magnetic coupling in the **c** direction is at the border between AFM and FM. Further studies of *R*FeAsO compounds with other *R* elements are necessary to determine whether this delicate balance in the magnetic coupling is controlled by steric effects or the magneto-crystalline anisotropy of the *R* element caused by crystal-electric field effects transferred through a complex coupling of the Nd and Fe magnetism. The proximity between the characteristic temperatures for the order-order transition of the Fe magnetic order at T^* to the onset of the Nd magnetic order at $T_{\mathrm{Nd}} \sim 6\,\mathrm{K}$ together with the common magnetic propagation at low temperatures suggests the second case as the more likely scenario.

Research at Ames Laboratory and Oak Ridge National Laboratory was supported by the U. S. Department of Energy, Office of Basic Energy Science, Division of Materials Sciences and Engineering and Scientific User Facilities Division, respectively. Ames Laboratory is operated for the U. S. Department of Energy by Iowa State University under Contract No. DE-AC02-07CH11358.

[1] Y. Kamihara, T. Watanabe, M. Hirano, and H. Hosono, J. Am. Chem. Soc. **130**, 3296 (2008).
[2] C. de la Cruz, Q. Huang, J. W. Lynn, J. Li, W. Ratcliff II, J. L. Zarestky, H. A. Mook, G. F. Chen, J. L. Luo, N. L. Wang, and P. Dai, Nature **453**, 899 (2008).
[3] A. S. Sefat, M. A. McGuire, B. C. Sales, R. Jin, J. Y. Howe, and D. Mandrus, Phys. Rev. B **77**, 174503 (2008).
[4] Z. A. Ren, J. Yang, W. Lu, W. Yi, G. Che, X. Dong, L. Sun, and Z. Zhao, Mater. Res. Innov. **12**, 105 (2008).
[5] Z.-A. Ren, J. Yang, W. Lu, W. Yi, X.-L. Shen, Z.-C. Li, G.-C. Che, X.-L. Dong, L.-L. Sun, F. Zhou, and Z.-X. Zhao, Europhys. Lett. **82**, 57002 (2008).
[6] G. F. Chen, Z. Li, D. Wu, G. Li, W. Z. Hu, J. Dong, P. Zheng, J. L. Luo, and N. L. Wang, Phys. Rev. Lett. **100**, 247002 (2008).
[7] Z.-A. Ren, G.-C. Che, X.-L. Dong, J. Yang, W. Lu, W. Yi, X.-L. Shen, Z.-C. Li, L.-L. Sun, F. Zhou, and Z.-X. Zhao, Europhys. Lett. **83**, 17002 (2008).
[8] J. Yang, Z.-C. Li, W. Lu, W. Yi, X.-L. Shen, Z.-A. Ren, G.-C. Che, X.-L. Dong, L.-L. Sun, F. Zhou, and Z.-X. Zhao, Supercon. Sci. Techol. **21**, 082001 (2008).
[9] J. W. G. Bos, G. B. S. Penny, J. A. Rodgers, D. A. Sokolov, A. D. Huxley, and J. P. Attfield, Chem. Commun. 3634 (2008).
[10] R. H. Liu, G. Wu, T. Wu, D. F. Fang, H. Chen, S. Y. Li, K. Liu, Y. L. Xie, X. F. Wang, R. L. Yang, L. Ding, C. He, D. L. Feng, and X. H. Chen, Phys. Rev. Lett. **101**, 087001 (2008).
[11] C. Wang, L. Li, S. Chi, Z. Zhu, Z. Ren, Y. Li, Y. Wang, X. Lin, Y. Luo, S. Jiang, X. Xu, G. Cao, and Z. Xu, Europhys. Lett. **83**, 67006 (2008).
[12] Y. Chen, J. W. Lynn, J. Li, G. Li, G. F. Chen, J. L. Luo, N. L. Wang, P. Dai, C. de la Cruz, and H. A. Mook, Phys. Rev. B **78**, 064515 (2008).
[13] Y. Qiu, W. Bao, Q. Huang, T. Yildirim, J. M. Simmons, M. A. Green, J. W. Lynn, Y. C. Gasparovic, J. Li, T. Wu, G. Wu, and X. H. Chen, Phys. Rev. Lett **101**, 257002 (2008).
[14] Q. Huang, J. Zhao, J. W. Lynn, G. F. Chen, J. L. Luo, N. L. Wang, and P. Dai, Phys. Rev. B **78**, 054529 (2008).
[15] D. H. Ryan, J. M. Cadogan, C. Ritter, F. Canepa, A. Palenzona, and M. Putti, Phys. Rev. B **80**, 220503(R) (2009).
[16] A. Marcinkova, D. A. M. Grist, I. Margiolaki, T. C. Hansen, S. Margadonna, and Jan-Willem G. Bos, Phys. Rev. B **81**, 064511 (2010).
[17] A. D. Christianson, E. A. Goremychkin, R. Osborn, S. Rosenkranz, M. D. Lumsden, C. D. Malliakas, I. S. Todorov, H. Claus, D. Y. Chung, M. G. Kanatzidis, R. I. Bewley, and T. Guidi, nature **456**, 930 (2008).
[18] J.-Q. Yan, S. Nandi, J. L. Zarestky, W. Tian, A. Kreyssig, B. Jensen, A. Kracher, K. W. Dennis, R. J. McQueeney, A. I. Goldman, R. W. McCallum, and T. A. Lograsso, Appl. Phys. Lett. **95**, 222504 (2009).
[19] P. Cheng, H. Yang, Y. Jia, L. Fang, X. Zhu, G. Mu, and H.-H. Wen, Phys. Rev. B **78**, 134508 (2008).
[20] A. A. Aczel, E. Baggio-Saitovitch, S. L. Bud'ko, P. C. Canfield, J. P. Carlo, G. F. Chen, P. Dai, T. Goko, W. Z. Hu, G. M. Luke, J. L. Luo, N. Ni, D. R. Sanchez-Candela, F. F. Tafti, N. L. Wang, T. J. Williams, W. Yu, and Y. J. Uemura, Phys. Rev. B **78**, 214503 (2008).
[21] Any mention of commercial products within this paper is for information only; it does not imply recommendation or endorsement by NIST.

[22] S. Nandi, M. G. Kim, A. Kreyssig, R. M. Fernandes, D. K. Pratt, A. Thaler, N. Ni, S. L. Budko, P. C. Canfield, J. Schmalian, R. J. McQueeney, and A. I. Goldman, Phys. Rev. Lett. **104**, 057006 (2010).

[23] J. A. Vrugt, C. J. F. ter Braak, C. G. H. Diks, B. A. Robinson, J. M. Hyman, and D. Higdon, Int. J. Nonlinear Sci. Numer. Simul. **10**, 273 (2009).

[24] J. Zhao, Q. Huang, C. de la Cruz, S. Li, J. W. Lynn, Y. Chen, M. A. Green, G. F. Chen, G. Li, Z. Li, J. L. Luo, N. L. Wang, and P. Dai, nature mat. **7**, 953 (2008).

[25] J. Zhao, Q. Huang, C. de la Cruz, J. W. Lynn, M. D. Lumsden, Z. A. Ren, J. Yang, X. Shen, X. Dong, Z. Zhao, and P. Dai, Phys. Rev. B **78**, 132504 (2008).

[26] S. A. J. Kimber, D. N. Argyriou, F. Yokaichiya, K. Habicht, S. Gerischer, T. Hansen, T. Chatterji, R. Klingeler, C. Hess, G. Behr, A. Kondrat, and B. Büchner, Phys. Rev. B **78**, 140503(R) (2008).

[27] S. Skanthakumar, H. Zhang, T. W. Clinton, W-H. Li, J. W. Lynn, Z. Fisk, and S.-W. Cheong, Physica C **160**, 124 (1989).

[28] J. W. Lynn, I. W. Sumarlin, S. Skanthakumar, W-H. Li, R. N. Shelton, J. L. Peng, Z. Fisk, and S-W. Cheong, Phys. Rev. B **41**, 2569 (1990).

[29] R. Sachidanandam, T. Yildirim, A. B. Harris, A. Aharony, and O. Entin-Wohlman, Phys. Rev. B **56**, 260 (1997).